Thermal dependent anharmonicity effects on gold bulk studied by extended x-ray-absorption fine structure

2009 J. Phys.: Condens. Matter 21 325404

(http://iopscience.iop.org/0953-8984/21/32/325404)

J. Phys.: Condens. Matter **21** (2009) 325404 (9pp) doi:10.1088/0953-8984/21/32/325404

Thermal dependent anharmonicity effects on gold bulk studied by extended x-ray-absorption fine structure

T Comaschi[1], **A Balerna**[2] **and S Mobilio**[1,2,3]

[1] Dipartimento di Fisica 'E Amaldi', Università Roma TRE, via della Vasca Navale 84, I-00146 Roma, Italy
[2] INFN-Laboratori Nazionali di Frascati, via E Fermi 40, I-00044 Frascati, Roma, Italy
[3] CNR—INFM c/o OGG European Synchrotron Radiation Facility ESRF, Grenoble, France

Received 1 April 2009, in final form 27 June 2009
Published 23 July 2009
Online at stacks.iop.org/JPhysCM/21/325404

Abstract
The structural parameters of the first five coordination shells of an Au bulk obtained from high accuracy L_3-edge extended x-ray absorption fine structure (EXAFS) spectra in the temperature range 20–300 K are reported. Good agreement with previously reported studies is found. The effective second and third order force constants evaluated using EXAFS data are compatible with those calculated from phonon dispersion curves. A careful comparison of the variations of the EXAFS first shell distance with x-ray diffraction data provided the mean squared relative displacement of the atomic vibrations perpendicular to the first interatomic bond. An alternative new approach that is useful in achieving this parameter when x-ray diffraction data are not available is proposed.

(Some figures in this article are in colour only in the electronic version)

1. Introduction

Very accurate temperature dependent extended x-ray absorption fine structure (EXAFS) measurements of bulk materials can give information on their general thermal properties and in particular on their thermal expansion coefficient. Thermal expansion is a direct fingerprint of the anharmonicity of the interatomic potential that gives rise to an increase in the average interatomic distance with temperature [1]. The main experimental method used to measure the thermal expansion of a solid at a microscopic level is x-ray diffraction, which directly provides the thermal behavior of the lattice parameters [2]. In some cases, like nanoparticles with very small dimensions (lower than 2 nm), such a method cannot be applied; in these cases EXAFS is the only way to get such information [3].

However, the evaluation of the thermal expansion from EXAFS data requires particular care, because specific effects due to the influence of the atomic vibrations perpendicular to the bond direction [4–6] must be taken into account.

As a matter of fact, EXAFS measures the thermal expansion of the average distance between neighboring atoms ('true thermal expansion', $\langle|\vec{r}_2 - \vec{r}_1|\rangle$) while Bragg diffraction measures the thermal behavior of the difference of average positions ('apparent bond expansion', $|\langle r_2\rangle - \langle r_1\rangle|$) [7]. The main difference between these two quantities is due to the atomic thermal vibrations perpendicular to the atomic bonds ($\Delta u_\perp$) [8–10]. There is no simple way to measure such a quantity, so up to now it has been determined by comparing the different thermal behaviors given by diffraction and EXAFS data. In order to get the true thermal expansion using only the EXAFS data an independent determination of $\Delta u_\perp$ is needed. Knowledge of $\Delta u_\perp$ is particularly important in some specific cases. There are some materials, like Si, Ge, some ceramics and zeolites with framework structures, that, in specific temperature ranges, show an unusual negative thermal expansion (NTE): an interatomic distance contraction in one or even in all directions as the temperature increases [11]. Experimental and theoretical studies on negative thermal expansion have been and are still being performed [8, 12–17]. Macroscopic thermal expansion is generally considered the resultant effect of two different competing contributions: a positive one connected to bond stretching and a negative one associated with a sort of geometrical tension effect. The last contribution is connected to the vibrational motions perpendicular to the bond direction and induces a contraction of the interatomic distances. In some cases such a contraction can prevail, giving rise to an overall NTE [18].

The aim of the present paper is to give an accurate determination of $\Delta u_\perp$ for Au bulk by comparing the thermal behavior of the interatomic distances given by x-ray diffraction and EXAFS; for this purpose very accurate experimental spectra and data analysis are needed. It will also be shown that in the present case a good estimation of $\Delta u_\perp$ can be achieved using a different procedure that does not require knowledge of the thermal expansion measured by x-ray diffraction. This method, based on symmetry considerations, can be very important in determining $\Delta u_\perp$ when diffraction data are not available, as in the case of very small particles.

The layout of the paper is as follows. Section 2 is dedicated to the description of some experimental details of the x-ray absorption measurements. In section 3 data analysis of the spectra is described. In section 4 the results of EXAFS analysis are presented. Sections 5 and 6 are respectively dedicated to the discussion of results and to the concluding remarks.

2. Experimental details

X-ray absorption spectra at the Au L_3 edge (11 919 eV) were recorded at the BM08 GILDA beamline of the European Synchrotron Radiation Facility (ESRF) at Grenoble (France) [19]. The electron energy and average current of the storage ring were 6 GeV and 190 mA, respectively. The sample was a gold foil of 99.97% purity and thickness 5 μm (purchased from Goodfellow Ltd). Two parallel silicon crystals with flat reflecting (311) faces, detuned to reduce the harmonics content, were used to monochromatize the x-ray beam. Spectra were recorded in transmission geometry, measuring the beam intensity before and after the sample with two ionization chambers filled with argon. Spectra were recorded in the temperature range from 20 up to 300 K, using a liquid helium cryostat; the sample was in a He gas atmosphere, and the preset temperature was controlled through an electric heater using a feedback loop. The average acquisition step between two energy points in the EXAFS region was 4 eV and the mean integration time was 3 s. At the highest temperatures two or even three spectra were measured to increase the signal to noise ratio.

3. Data analysis

EXAFS spectra were extracted from the raw data according to standard procedures [20]. As a first step a straight line was subtracted from all spectra by best fitting the pre-edge region. The threshold energy E_0 was determined as the maximum of the first derivative of each spectrum in the near-edge region. All spectra were aligned to have within 0.1 eV the same E_0 value of the lowest temperature spectrum; this procedure is necessary for high accuracy data analysis, because a 0.1 eV shift in the edge position results in a shift of 0.001 Å in interatomic distances. The values of the photoelectron wavenumber k were calculated from the energy origin E_0 as

$$k = \sqrt{\frac{2m}{\hbar^2}(E - E_0)}. \qquad (1)$$

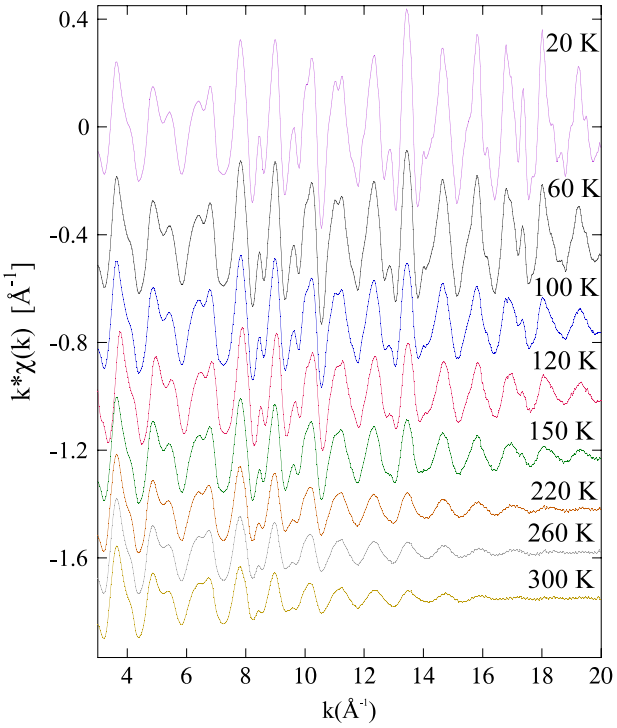

Figure 1. EXAFS signals at different temperatures for gold bulk.

The EXAFS signal was determined as $\chi(k) = [\mu(k) - \mu_1(k)]/\mu_0(k)$, where $\mu(k)$ is the experimental absorption coefficient; $\mu_1(k)$ is a spline polynomial best fitting the average behavior of $\mu(k)$; $\mu_0(k)$ is the smooth polynomial function $(\mu_0(k) = \frac{J}{d}(1 - \frac{8}{3}k^2a^2))$, that theoretically describes the monotonic decrease of the atomic absorption coefficient; d is the thickness of the sample; the scaling factor J is determined by normalizing $\mu_0(k)$ to the experimental absorption at the edge [21]. The EXAFS spectra multiplied by k are shown in figure 1.

The $k^2\chi(k)$ signals were Fourier transformed in the range $k = 2.5$–19 Å^{-1}. A Gaussian window was used in the transformation. The corresponding curves in r space are shown in figure 2; it can be clearly noticed how the magnitude of the Fourier transform (FT) decreases with increasing temperature. Once given the fcc structure of gold bulk, the assignment of the Fourier peaks is straightforward. The first peak, centered at about 2.75 Å, is due to the 12 first neighbors in the fcc structure; it is well isolated at all temperatures from the other peaks, so its contribution can be singled out by a back-Fourier transform. The other peaks correspond to the outer coordination shells; they are quite well separated at low temperatures but progressively merge at increasing temperatures. They are due to the superposition of single scattering (SS) as well as to non-negligible multiple scattering (MS) contributions.

The quantitative data analysis of the first coordination shell was performed through the method of phase difference and amplitude ratio [5, 22]; as a matter of fact MS effects do not contribute to the first coordination shell signal and the ratio method gives the best possible accuracy. It consists in the separate analysis of phases and amplitudes of the filtered

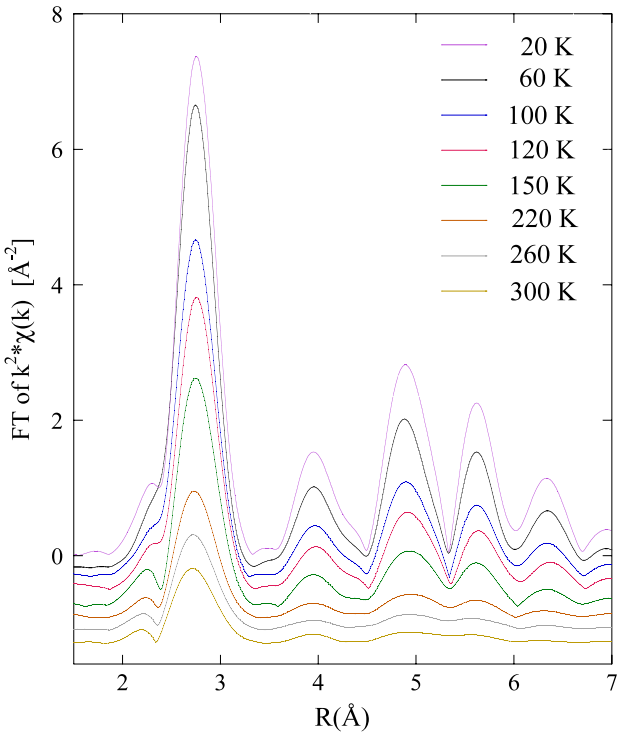

Figure 2. Fourier transforms of EXAFS signals at different temperatures.

EXAFS signal; as is well known [20], the inverse FT of the first shell signal given by

$$k\chi(k) = A(k)\sin\Phi(k) \tag{2}$$

provides the generalized amplitude $A(k)$ and phase $\Phi(k)$ functions of the first shell oscillating EXAFS signal. Both functions contain terms originating from the scattering of the photoelectrons and from the structural parameters of the first coordination shell. In the harmonic approximation the radial distribution function of atoms around the absorber is well described by a Gaussian distribution; in this case the phase and the amplitude functions are given by

$$\Phi(k) = 2kR + \phi(k) \tag{3}$$

$$A(k) = S_0^2 NA(k)\mathrm{e}^{-2R/\lambda}\mathrm{e}^{-2\sigma^2k^2} \tag{4}$$

where R, N and σ^2, respectively, stand for the distance, coordination number and Debye–Waller factor of the shell under consideration (the first coordination shell in the present case) and are the structural parameters to be determined. S_0^2, $\phi(k)$, λ and $A(k)$ are non-structural functions and parameters arising from the physical origin and from the characteristics of the EXAFS process. In order to eliminate these terms a reference spectrum of a model compound is needed and the first shell interatomic distance and the coordination number are calculated from the amplitude and phase function of the sample ($\Phi_s(k)$ and $A_s(k)$) and of the reference compound spectra ($\Phi_r(k)$ and $A_r(k)$).

Under the hypothesis that the scattering terms are identical for the sample and for the reference compound, these calculated functions depend only on the structural parameters of the specific coordination shell. In the harmonic approximation it can be shown that [20]

$$\frac{\Phi_s(k) - \Phi_r(k)}{2k} = (R_s - R_r) \tag{5}$$

$$\ln\frac{A_s(k)}{A_r(k)} = -2k^2(\sigma_s^2 - \sigma_r^2) + \ln\left(\frac{N_s(k)}{N_r(k)}\right). \tag{6}$$

When the distribution function is non-Gaussian, the effective distribution of distances measured by EXAFS ($P(r,k,T) = \rho(r,T)\exp[-2r/\lambda(k)]/r^2$) can be expanded in cumulants [23] as

$$\int_0^\infty P(r,k,T)\mathrm{e}^{2\mathrm{i}kr}\,\mathrm{d}r = \mathrm{e}^{[\sum_0^\infty[\frac{(2\mathrm{i}k)^n C_n(k,T)}{n!}]]} \tag{7}$$

where C_1 is the mean value of the interatomic distance, C_2 is the root mean square of the interatomic distances, C_3 is the asymmetry of the distribution and C_4 describes symmetric deviations from the Gaussian shape; higher order cumulants can be generally neglected. In this approximation the EXAFS function $\chi(k)$ becomes:

$$\chi(k) = \frac{S_0^2}{kR^2}NF(k)\mathrm{e}^{(C_0 - 2C_2k^2 + \frac{2}{3}C_4k^4 + \cdots)} \times \sin\left(2kC_1 - \tfrac{4}{3}C_3k^3 + \cdots + \phi(k)\right). \tag{8}$$

Taking into account terms up to the fourth order, equations (5) and (6) become

$$\frac{\Phi_s(k) - \Phi_r(k)}{2k} = \Delta C_1 - \frac{2}{3}k^2\Delta C_3, \tag{9}$$

$$\ln\frac{A_s(k)}{A_r(k)} = -2k^2\Delta C_2 + \frac{2}{3}k^4\Delta C_4 \tag{10}$$

where the ΔC_i are the differences between the ith cumulant expansion coefficients of the studied and of the reference sample. In equation (10) the coordination number was assumed constant ($N = 12$ in our case).

The typical curves related to phase differences and logarithms of amplitude ratios obtained from the performed data analysis are shown in figure 3; the lowest temperature spectrum recorded at 20 K was used as a reference. These plots allow us to evaluate the overall quality of the experimental data as well as the useful k range.

According to equation (9) the phase difference, divided by k and plotted against k^2, should show a linear behavior; its crossing point with the y-axis and its slope give the difference of the first and third cumulants ΔC_1 and ΔC_3, respectively. In the figure we also show the best fits with a straight line, that give the numerical values for ΔC_1 and ΔC_3. The increase of both quantities from 20 to 300 K is immediately evident. In a similar way ΔC_2 and ΔC_4 were determined from the plot of the logarithms of the amplitude ratios.

The uncertainties were estimated by varying the fitting ranges. The values of the fourth cumulant are not reported in in table 1 because at all temperatures an F-test between the fits performed with and without C_4 has shown that it can be neglected. To check these first shell results we

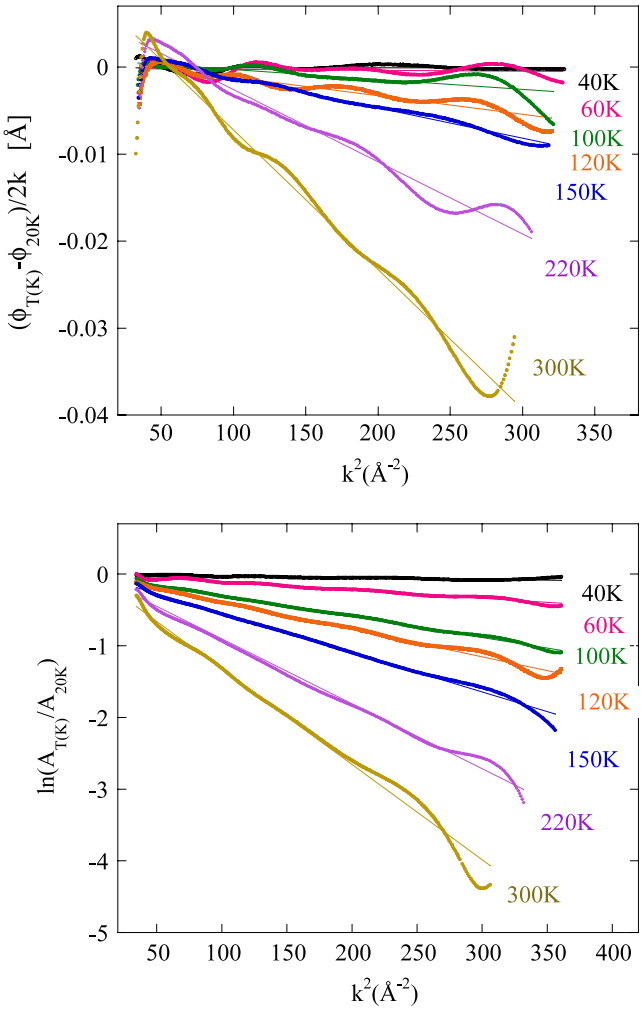

Figure 3. Plot of the difference of phases (upper panel) and of the logarithm of the amplitude ratio (lower panel) as a function of the square of the wavevector at different temperatures.

analyzed the same data using a second procedure. The inverse FTs of the first coordination shell at all temperatures were simulated using theoretical amplitudes and phases provided by the FEFF8 code [24]; the simulation was then best fitted to the experimental spectra. In a first run, six free parameters were fitted, namely the first four cumulants C_1–C_4, the amplitude reduction factor S_0^2, which takes into account the intrinsic photoelectron inelastic scattering, and ΔE_0, the edge energy mismatch between theory and experiment. Then in a second run these last two parameters were fixed at the values of 0.97 and 8.0 eV, respectively, at all temperatures; these values are the mean values found in the first run for all the spectra. In this way we minimized the number of free parameters in the fit [17]. This procedure allowed us to determine the absolute values of the cumulant coefficients; the values relative to the $T = 20$ K spectrum of the cumulant coefficients found with the two different approaches turned out to be in very good agreement, but, as expected, the first procedure provided a higher accuracy. The absolute values of the first three polynomial coefficients $C_n(T)$ so obtained are reported in table 1.

Table 1. Values of the first three cumulants of the effective distribution as a function of T for the first coordination shell of gold bulk.

Au foil			
T (K)	C_1 (Å)	C_2 (10^{-2} Å^2)	C_3 (10^{-3} Å^3)
20	2.8760(5)	0.170(2)	−0.0380(8)
40	2.8759(5)	0.182(2)	−0.0383(8)
60	2.8758(5)	0.226(2)	−0.0366(7)
70	2.8762(5)	0.242(3)	−0.0325(6)
80	2.8764(6)	0.269(2)	−0.0267(7)
100	2.8769(6)	0.318(2)	−0.0212(7)
120	2.8769(7)	0.362(3)	−0.0064(7)
150	2.8783(7)	0.444(3)	0.014(8)
160	2.8789(7)	0.461(3)	0.021(8)
180	2.8794(7)	0.474(3)	0.034(7)
200	2.8794(6)	0.552(3)	0.046(7)
220	2.8817(7)	0.622(2)	0.086(7)
245	2.8812(7)	0.667(3)	0.104(7)
260	2.8822(7)	0.721(3)	0.128(7)
270	2.8825(7)	0.718(3)	0.146(7)
290	2.8824(8)	0.795(3)	0.172(7)
300	2.8849(7)	0.834(3)	0.203(8)

The signals of the higher coordination shells are well visible in the Fourier transformed spectra of figure 2 above 3 Å; as underlined above, they originate both from SS and MS contributions. For these shells MS paths are relevant and cannot be neglected in an accurate data analysis, because in the fcc structure atoms are arranged in a nearly collinear geometry. To properly take into account MS contributions, the outer shells were analyzed through the best fitting of simulated spectra built up using theoretical phases and amplitudes provided by the FEFF8 code. For these higher order coordination shells the standard EXAFS formula was used, which implies a Gaussian distribution function as usually performed [25, 26]. All SS and MS paths were considered up to the fifth coordination shell. The spectra were fitted both in k-space and in r-space, including in this case FT-peaks up to about 7 Å. To reduce the number of fitting parameters the following precautions were taken: (a) all first shell parameters were fixed to the values obtained from the first shell analysis; (b) the bond lengths of the higher order shells were all linked to that of the second sphere according to a fcc structure; (c) coordination numbers were fixed to the fcc structure values; (d) for MS paths the same distance for the corresponding SS paths was used. Also in this case the numerical values of S_0^2 and ΔE_0 were fixed using the same procedure as for the first shell.

Quite a good match between experiment and theory was obtained both in k and in R space, as shown in figures 4 and 5. The values obtained at 20 K are reported in table 2.

4. Results

4.1. First coordination shell data analysis

The first coordination shell EXAFS analysis, previously described, provided the temperature dependence of the first three cumulants C_i. As is well known, EXAFS does not probe the true real pair distribution function $\rho(r, T)$ but an effective

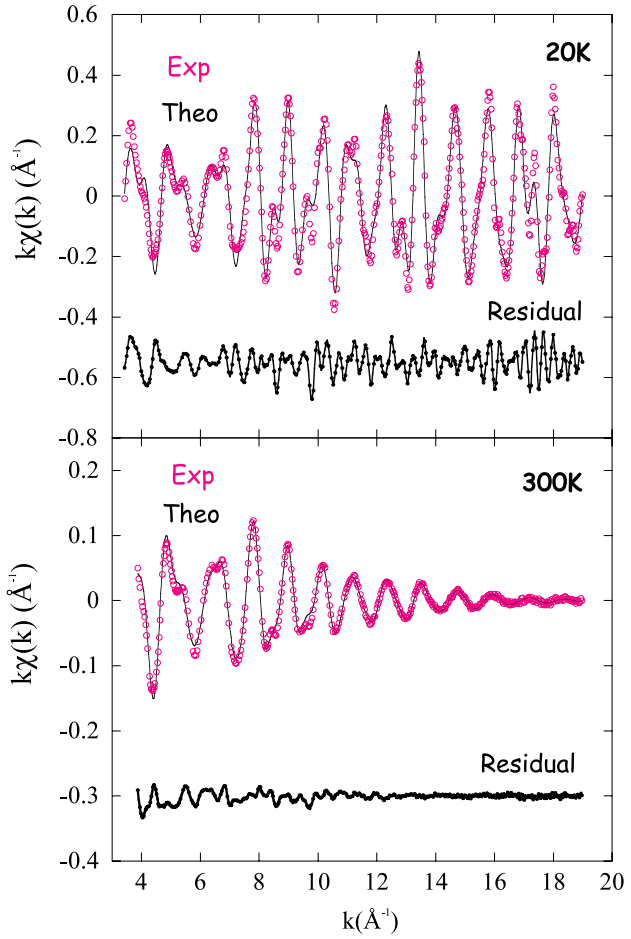

Figure 4. Experimental EXAFS signals of Au bulk at 20 K (upper panel) and 300 K (lower panel) and best fit simulated signals (continuous line). Also the differences between theoretical and experimental signals (residual) are reported. The oscillating residual achieved for the 20 K EXAFS signal is due to higher order coordination shells (bigger than five) not included in the analysis which give a significant contribution to the experimental $\chi(k)$ signal.

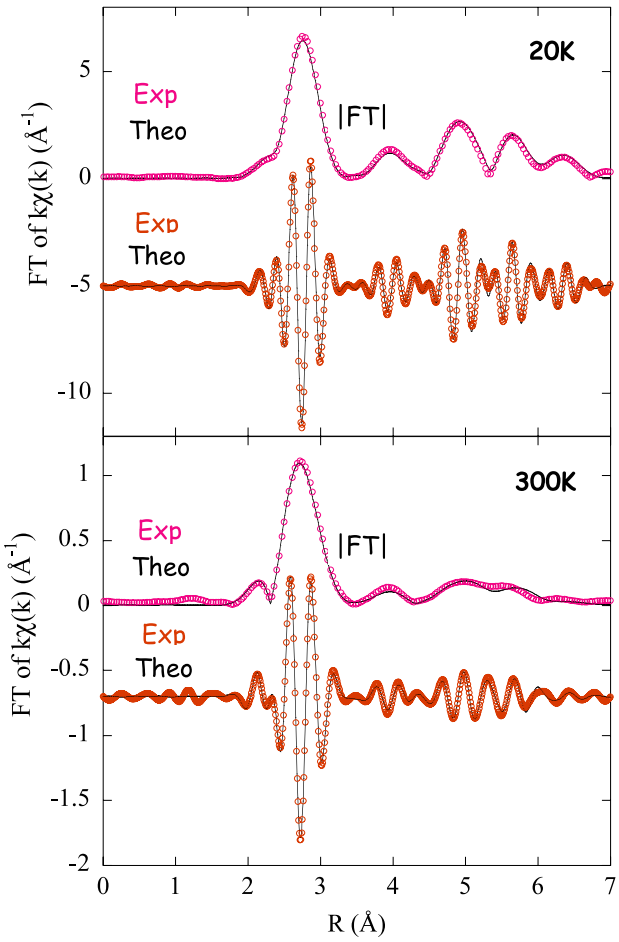

Figure 5. Amplitudes and imaginary parts of the Fourier transforms of the experimental signals at 20 K (upper panel) and 300 K (lower panel) and the best fitting simulated signals (continuous line).

Table 2. Coordination numbers (N), distances (R) and Debye–Waller factors (σ^2) of five higher coordination shells of Au bulk at 20 K.

Shell	N	R (Å)	σ^2 (10^{-2} Å^2)
II	6.0 (fixed)	4.069(7)	0.220(7)
III	24.0 (fixed)	4.984(7)	0.242(7)
IV 2-body	12.0 (fixed)	5.755(7)	0.286(7)
IV 3-body	24.0 (fixed)	5.755(7)	0.277(7)
IV 4-body	12.0 (fixed)	5.755(7)	0.267(7)
V	24.0 (fixed)	6.434(7)	0.287(7)

one ($P(r, \lambda)$), given by

$$P(r, \lambda, T) = \rho(r, T)\frac{e^{-2r/\lambda}}{r^2} \tag{11}$$

where λ is the mean free path of the photoelectron. The correcting terms arise from the damping of the primary photoelectron for the inelastic losses and for the finite lifetime of the core–hole and from the decrease of the photoelectron wavefunction at increasing distances from the absorbing atom. Accordingly the cumulant coefficients C_i provided by the above described analysis are those of the effective pair distribution function. It has been demonstrated [6, 27] that the cumulant coefficients of the real distribution function, C_i^*, are well approximated by those of the effective distribution, C_i, just excluding C_1^* which is given by

$$C_1 = C_1^* - \frac{2C_2^*}{C_1^*}\left(1 + \frac{C_1^*}{\lambda}\right). \tag{12}$$

Starting from the values of C_1 and C_2^* we calculated C_1^* assuming different values (6, 9 and 12 Å) for λ; the spread of the obtained values was very small, less than uncertainties.

In figure 6 we report the temperature dependence of the mean values of the interatomic distances obtained from the effective distribution compared with that of the real distribution calculated using equation (12).

It can be noted that the difference between the two is small but appreciable: it amounts approximately to 0.01 Å at 300 K. In the same figure we show also the first shell crystallographic thermal expansion measured by x-ray diffraction. The small difference between diffraction and EXAFS data shows why very accurate spectra and data analysis are needed to observe this effect.

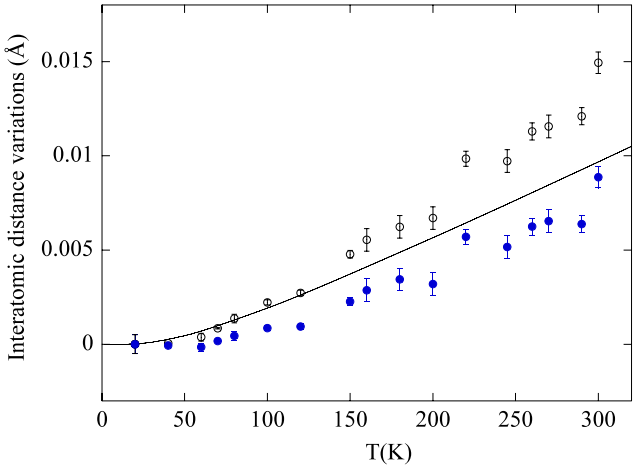

Figure 6. Temperature behavior of the Au first shell interatomic distance of the effective (full circles) and of the real distribution ($\lambda = 9$ Å) (empty circles). The values are relative to the $T = 20$ K spectrum; the continuous line is the crystallographic thermal expansion.

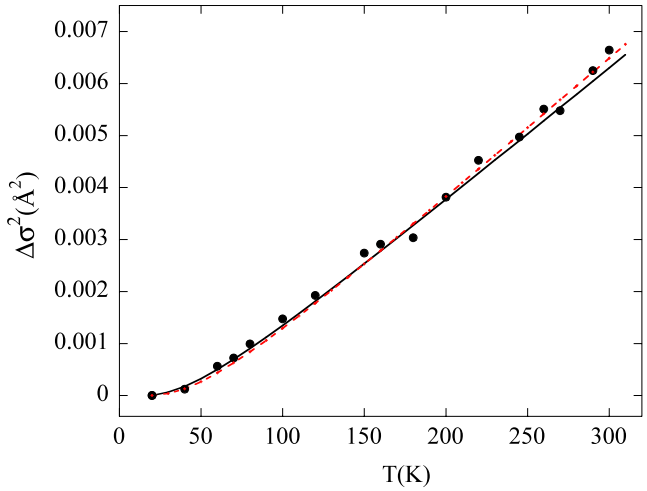

Figure 7. Temperature behavior of the Au first shell Debye–Waller factor $\Delta\sigma^2$ relative to the $T = 20$ K spectrum, obtained from the ratio method. The black line is the best fit with an Einstein model while the dashed line is the fit with a correlated Debye model.

In figure 7 the thermal behavior of the second cumulants ΔC_2^*, generally known as the Debye–Waller factor and indicated as $\Delta\sigma^2$, relative to the $T = 20$ K spectrum, is shown. The present value are in excellent agreement with the literature [28–30]; they are slightly different from those we reported in previous papers [31, 32], mainly because of the actual higher data quality. It is well known that the EXAFS Debye–Waller factor is sensitive to both structural and thermal disorder. Since the structural disorder is constant with temperature, the thermal disorder can be isolated from the thermal behavior of the Debye–Waller factors. This thermal contribution provides information on the dynamical properties of the absorber–backscatterer pair, namely on the effective bond stretching force constant between them, and can be used to determine the strength of the chemical bonds [33]. For this purpose we performed a fitting of the experimental data with an Einstein model [9]; the agreement found between the theoretical model and the experimental data was excellent (figure 7). The so obtained Einstein frequency ω_E was 17.7 THz, in very good agreement with previous results [34].

In a quantum single oscillator approximation, the oscillator mean frequency $\bar{\omega}$ is related to the second order effective force constant k_0 by $k_0 = \mu\bar{\omega}^2$ (where μ is the reduced mass) [33, 35]. The Einstein frequency obtained from the data, that gives the inverse second moment of the vibrational phonon spectrum, can be used to determine the mean frequency $\bar{\omega}$ as

$$\bar{\omega}^2 = \eta\omega_E^2 \tag{13}$$

provided the factor η is known [36]. To our knowledge no evaluation of η exists for Au; Vila *et al* [36] reported the value of $\eta = 0.73$ for Cu, estimated using the Lanczos algorithm with the LDA prescription for the dynamical matrix. Assuming that such a value is also valid for Au, which, like Cu, has a fcc structure, we achieve $\bar{\omega} = 12.9$ THz; from such a value of $\bar{\omega}$ we get $k_0 = 2.35$ eV Å^{-2} $= 37.6$ N m^{-1}. This value is in excellent agreement with that estimated [37] from the experimental phonon dispersion curves of gold bulk $k_0 = 39.9$ N m^{-1}.

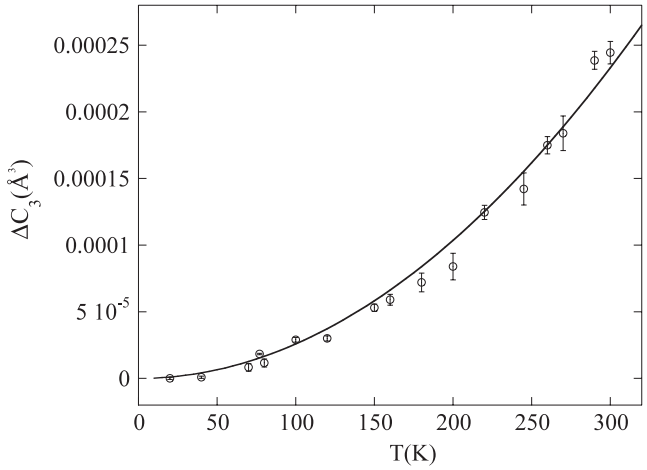

Figure 8. Temperature dependence of the third cumulant relative to the $T = 20$ K value; the continuous line is the best fit using the theoretical model (equation (14)).

The fitting of the same data with a Debye correlated model (also shown in figure 7), gave a value for the Debye temperature of $\Theta_D = 180 \pm 4$ K; such a value is in agreement with the values recently reported in literature where it is shown that the Au Debye temperature ranges from 165 K at low T to nearly 190 K at high T [38–40].

Figure 8 reports the relative values of the third cumulant obtained from the data analysis approach used here. Below 100 K the values are very small but different from zero due to quantum effects and to the zero point motion; above 100 K the values are no longer negligible and grow with temperature, showing how the effective distribution progressively deviates from a Gaussian approximation. According to the above quoted quantum models [33, 35], to leading order in k_3 the

thermal behavior of the third cumulant is given by

$$C_3^*(T) = -\frac{2k_3(\sigma_0)^4}{k_0}\frac{z^2+10z+1}{(1-z)^2} + C_3^*(0) \qquad (14)$$

where $\sigma_0^2 = \frac{\hbar}{2\mu\omega}$ and $z = e^{-\frac{\hbar\omega}{KT}}$.

A best fit of the experimental data to this equation, assuming for k_0 the values reported above, gave for the third order force constant a value of $k_3 = -3.1 \times 10^{11}$ N m^{-2}, in quite good agreement with the value obtained from the dispersion curves [41] of Au bulk ($k_3 = -3.6 \times 10^{11}$ N m^{-2}).

4.2. Higher order coordination shells

The ratio between the distances of shells II and I was calculated, and within the experimental errors it is equal to $\sqrt{2}$, as expected for a fcc structure.

The Debye–Waller factors of the next neighboring shells were fitted with a correlated Debye model; the Debye temperature values obtained (170 K) are consistent with that of the first shell. It is worth noting that the fourth shell data are characterized by a large correlation between the values of the single scattering and multiple scattering σ^2s used to fit this shell.

5. Discussion

The difference between the thermal expansion measured by EXAFS and by x-ray diffraction, shown in figure 6, is rather small but not negligible and comes mainly from the different effect of the atomic thermal vibrations on the structural parameters measured by the two techniques, i.e. the interatomic distance and the crystallographic lattice parameter, respectively.

As a matter of fact, EXAFS spectra are sensitive to the distances between atoms and atomic vibrations change these interatomic distances. A relevant parameter is the mean square of the relative distance generally indicated as MSRD:

$$\text{MSRD} = \langle \Delta u^2 \rangle = \langle |\vec{R}_1 - \vec{R}_2|^2 \rangle \qquad (15)$$

where R_1 and R_2 are the crystallographic positions of atoms 1 and 2. Once fixed for a couple of atoms, the MSRD can be decomposed into two components, one parallel ($\Delta u_\parallel$) and one perpendicular ($\Delta u_\perp$) to the interatomic distance. To first order $\langle (\Delta u_\parallel)^2 \rangle$ does not change the mean interatomic distance; it is equal to the Debye–Waller factor σ^2 and, as stressed above, it carries information on the dynamical properties of the atomic motion. Knowledge of $\langle (\Delta u_\parallel)^2 \rangle$ is required to determine the cumulant of the real distribution function C_1^* from the effective one C_1.

On the other hand, the perpendicular MSRD, $\langle (\Delta u_\perp)^2 \rangle$, changes the mean value of the interatomic distance and is responsible of the difference between the values measured by EXAFS and by diffraction [4]:

$$R_{\text{Exafs}} = R_{\text{Diffraction}} + \frac{\langle (\Delta u_\perp)^2 \rangle}{2R_{\text{Diffraction}}}. \qquad (16)$$

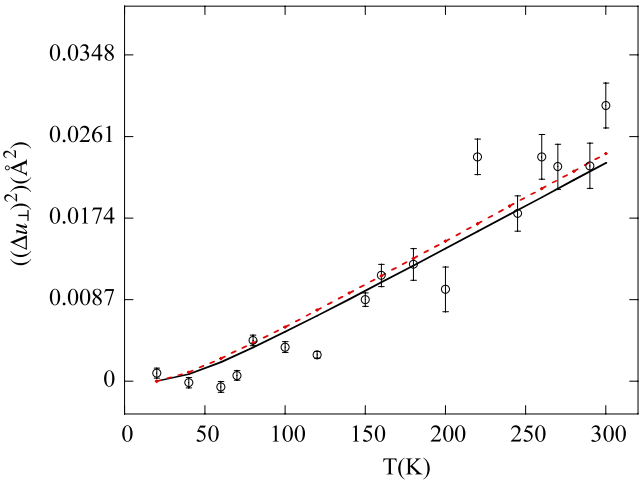

Figure 9. Thermal behavior of $\langle \Delta u_\perp^2 \rangle$ evaluated from equation (16). The continuous line is the best fit according to a Debye correlated model while the dashed one is the best according to an Einstein model.

No experimental technique can measure this quantity directly, so it can be obtained only from the previous equation (figure 9). In principle $\langle (\Delta u_\perp)^2 \rangle$ gives relevant information on the eigenvectors of the dynamical matrix additional to that provided by the parallel MRSD. Moreover it is a crucial quantity for clarifying the tension effect, which is claimed to be the origin of NTE in many systems [42].

The fit of the perpendicular $\langle (\Delta u_\perp)^2 \rangle$ with an Einstein model gives the Einstein frequency for vibrational modes perpendicular to the first shell interatomic distance, i.e. perpendicular to the (110) direction and to all the other equivalent directions. The value found is $(\omega_E)_\perp = 13.6$ THz, i.e. $(\omega_E^\perp/\omega_E^\parallel)_{\text{exp}} = 0.77$.

Within the Einstein model, the ratio between the Einstein frequencies for perpendicular and radial motion is given by

$$\frac{\omega_E^\perp}{\omega_E^\parallel} = \frac{2}{\gamma}\cdot\frac{\coth(\beta\hbar\omega_E^\perp/2)}{\coth(\beta\hbar\omega_E^\parallel/2)} \simeq \frac{2}{\gamma} \qquad (17)$$

at high temperature. Here γ is the ratio between the perpendicular and parallel components of the MSRD, $\gamma = \frac{\langle \Delta u_\perp^2 \rangle}{\langle \Delta u_\parallel^2 \rangle}$; it measures the anisotropy of the relative vibrations. Vila *et al* [36] showed that, assuming a simple model based on a single spring constant, γ is only weakly dependent on the temperature and that at high temperature in fcc crystals it amounts to $\frac{5}{2}$. Using such a value in equation (17) we get

$$\frac{\omega_E^\perp}{\omega_E^\parallel} = \frac{2}{2.5} = 0.8 \qquad (18)$$

in very good agreement with our experimental value.

An alternative way to justify the ratio $(\omega_E^\perp/\omega_E^\parallel)_{\text{exp}} = 0.77$ is to consider that provided the above introduced factor η is the same for parallel and perpendicular motions, the same ratio 0.77 also holds for the mean frequencies of the oscillations parallel $\bar{\omega}^\parallel$ and perpendicular $\bar{\omega}^\perp$ to the (110) direction. For the high symmetry of the Au crystal, we can also assume

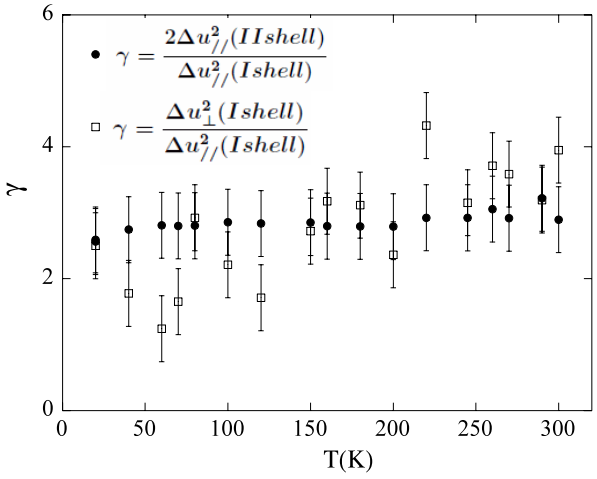

Figure 10. Thermal behavior of the experimental ratio $\frac{\langle \Delta u_\perp^2 \rangle}{\langle \Delta u_\parallel^2 \rangle}$ obtained from data of figures 9 and 7 (empty squares) and from equation (21) (full circles).

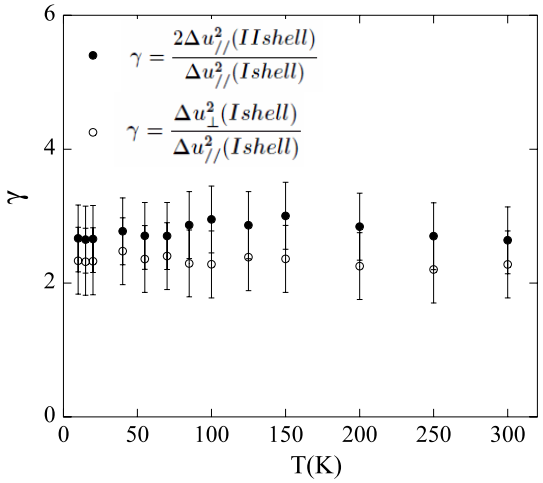

Figure 11. Thermal behavior of the experimental ratio $\frac{\langle \Delta u_\perp^2 \rangle}{\langle \Delta u_\parallel^2 \rangle}$ obtained for Cu (data were taken from [8]) according to the two different procedures of calculation used also in the case of Au.

that the mean values of the atomic movements parallel and perpendicular to the (110) first neighbors direction can be well approximated by the mean value of the phonon frequencies of longitudinal $\bar{\omega}^{\mathrm{L}}$ and transverse $\bar{\omega}^{\mathrm{T}}$ phonons propagating in the same direction. For this reason we calculated the mean value of the frequencies of the longitudinal and transverse branches of the (110) direction from experimental dispersion curves [38], also obtaining in this case the value $(\bar{\omega}^{\mathrm{T}}/\bar{\omega}^{\mathrm{L}})_{\mathrm{theor}} = 0.77$.

In figure 10 we report the experimental values we have found for the γ ratio. The data are rather scattered, but their mean value is significantly higher than 2.5 ($\bar{\gamma} = 2.78$). Such a value indicates the presence of an anisotropy higher than that foreseen on the basis of the mono-dimensional single force constant oscillator and due essentially to the presence of many non-independent oscillators. Our experimental value is similar to those previously obtained for other fcc metals [8, 36, 43]. Fornasini *et al* [8] estimated for Cu a ratio between 2 and 3 in a temperature range up to 500 K in agreement with path integral Monte Carlo simulations, which gives a value of 2.7 [44]. Vila *et al* [36] reported a value between 2.17 and 2.5 calculated on the basis of density functional theory; finally Haug *et al* [43] in crystalline Ag experimentally found a value of 2.2 ± 0.7.

Due to the relevance of this parameter for determining the anisotropy of the relative atomic vibrations in the perpendicular and parallel directions and taking into account that it is not always possible to obtain x-ray diffraction data, we propose here a different procedure to evaluate γ. In the present case $\langle \Delta u_\perp^2 \rangle$ indicates the MSRD of the atomic vibration perpendicular to the first shell interatomic bond, i.e. perpendicular to the (110) direction. The high symmetry of the fcc lattice states that all directions perpendicular to (110) one are equivalent, so we can choose one of them to evaluate $\langle \Delta u_\perp^2 \rangle$. Choosing the (001) direction, which is also the direction of the second shell, we have that

$$\langle \Delta u_\perp^2(110) \rangle = 2\langle \Delta u_\parallel^2(001) \rangle \tag{19}$$

i.e.

$$\langle \Delta u_\perp^2(\mathrm{I\ shell}) \rangle = 2\langle \Delta u_\parallel^2(\mathrm{II\ shell}) \rangle. \tag{20}$$

On the basis of this relation, we conclude that it is possible to evaluate γ as

$$\gamma = \frac{2\langle \Delta u_\parallel^2(\mathrm{II\ shell}) \rangle}{\langle \Delta u_\parallel^2(\mathrm{I\ shell}) \rangle}. \tag{21}$$

The values found using this procedure are indicated by the full circles in figure 10. The result is quite good: γ has again a mean value of 2.78 (higher than 2) and in addition data are not as scattered as when using the previous procedure. We conclude that, at least in the present case, this second procedure to evaluate γ is reliable and consequently gives a way to determine $\langle (\Delta u_\perp)^2 \rangle$ without knowledge of $R_{\mathrm{Diffraction}}$. We recall here that knowledge of $\langle (\Delta u_\perp)^2 \rangle$ is very important both to clarify the tension effects in NTE materials and to determine the crystallographic expansion coefficient from the thermal behavior of the interatomic distances of EXAFS data. Both aspects are of relevance in systems like very small clusters, where diffraction spectra are difficult to measure.

To check the validity of the above described method to determine $\langle (\Delta u_\perp)^2 \rangle$ in other systems we used the same procedures on the data of metallic copper reported in [8]. As shown in figure 11 in this case as well the two methods provide results that are in good agreement, showing how in systems of high symmetry the proposed alternative method for determining $\langle (\Delta u_\perp)^2 \rangle$ is reliable.

6. Conclusions

We have shown how the coupling of high quality EXAFS spectra recorded at third generation synchrotron radiation facilities with highly accurate data analysis methods allows one to obtain relevant physical information on the structural and dynamical properties of interatomic bonds from EXAFS spectra. In particular, as already shown in other systems, comparison of the thermal behavior of the first shell bond distance with the thermal expansion obtained from x-ray

diffraction data provided the mean squared relative amplitude of atomic vibrations perpendicular to the bond length, which is a relevant quantity for fully understanding tension effects. The alternative method to evaluate such a quantity based only on EXAFS data, proposed in the present paper, is relevant in all those systems where x-ray diffraction measurements cannot be easily performed. More investigations are needed to check both the validity of the proposed method in systems with symmetries different from the fcc one and its applicability to the study of very low-dimensional nanoparticles, where x-ray diffraction data are usually not available.

Acknowledgments

We thank Carlo Meneghini for the useful hints during the XAS data analysis, Chiara Maurizio for her precious help in experimental data acquisitions in the first stage of this research and Francesco D'Acapito for many stimulating discussions. We gratefully acknowledge the support of GILDA technical staff (F d'Anca, F La Manna, V Sciarra, V Tullio) in this research. GILDA is financed by the Italian Institutions CNR, INFM and INFN.

References

[1] Ashcroft N W and Mermin N D 1976 *Solid State Physics* (Philadelphia, PA: Saunders)
[2] Warren B E 1990 *X-Ray Diffraction* (Reading, MA: Addison-Wesley)
[3] Comaschi T, Balerna A and Mobilio S 2008 *Phys. Rev.* B **77** 075432
[4] Fornasini P 2001 *J. Phys.: Condens. Matter* **13** 7859
[5] Dalba G and Fornasini P 1997 *J. Synchrotron Radiat.* **4** 243
[6] Fornasini P, Monti F and Sanson A 2001 *J. Synchrotron Radiat.* **8** 1214
[7] Busing W R and Levy H A 1964 *Acta Crystallogr.* **17** 142
[8] Fornasini P, Beccara S a, Dalba G, Grisenti R, Sanson A, Vaccari M and Rocca F 2004 *Phys. Rev.* B **70** 174301
[9] Dalba G, Fornasini P, Grisenti R and Purans J 1999 *Phys. Rev. Lett.* **82** 4240
[10] Dalba G, Fornasini P and Gotter R 1995 *Phys. Rev.* B **52** 149
[11] Adenstedt H 1936 *Ann. Phys., Lpz.* **26** 69
[12] Collins J G and Whit G K 1964 *Prog. Low Temp. Phys.* **4** 450
[13] Barron T H K 1970 *J. Appl. Phys.* **41** 5044
[14] Barron T H K and White G K 1999 *Heat Capacity and Thermal Expansion at Low Temperature* (Dordrecht: Kluwer)
[15] Barron T H K, Collins J G and White G K 1980 *Adv. Phys.* **29** 609
[16] Goodwin A L, Calleja M, Conterio M T, Dove M T, Evans J S O, Keen D A, Peters L and Tucker M G 2008 *Science* **319** 794
[17] Vaccari M, Grisenti R, Fornasini P, Rocca F and Sanson A 2007 *Phys. Rev.* B **75** 184307
[18] Barrera G D *et al* 2005 *J. Phys.: Condens. Matter* **17** R217
[19] http://www.esrf.eu/UsersAndScience/Experiments/CRG/BM08/
[20] Lee P A, Citrin P H, Eisenberger P and Kincaid B M 1981 *Rev. Mod. Phys.* **53** 769
[21] Lengeler B and Eisenberger P 1980 *Phys. Rev.* B **21** 4507
[22] Martens G, Rabe P, Schwentner N and Werner A 1977 *Phys. Rev. Lett.* **39** 1411
[23] Bunker G 1983 *Nucl. Instrum. Methods Phys. Res.* **207** 437
[24] Ankudinov A, Ravel B, Rehr J and Conradson S 1998 *Phys. Rev.* B **58** 7565
[25] Lee P A and Pendry J B 1975 *Phys. Rev.* B **11** 2795
[26] Rehr J J and Alberts R C 2000 *Rev. Mod. Phys.* **72** 621
[27] Yokoyama T, Ohta T and Sato H 1997 *Phys. Rev.* B **55** 11320
[28] Lutzenkirchen-Hecht D and Frahm R 2000 *Physica* B **283** 108
[29] Kluth P, Johannessen B, Araujo L L and Ridgway M C 2007 *AIP Conf. Proc.* **882** 731
[30] Marcus M A, Andrews M P, Zegenhagen J, Bommannavar A S and Montano P 1990 *Phys. Rev.* B **42** 3312
[31] Balerna A, Bernieri E, Picozzi P, Reale A, Santucci S, Burattini E and Mobilio S 1985 *Phys. Rev.* B **31** 5058
[32] Balerna A and Mobilio S 1986 *Phys. Rev.* B **34** 2293
[33] Frenkel A I and Rehr J J 1993 *Phys. Rev.* B **48** 585
[34] Knapp G S, Pan H K and Tranquada J M 1985 *Phys. Rev.* B **32** 2006
[35] Yokoyama T 1998 *Phys. Rev.* B **57** 3423
[36] Vila F D, Rehr J J, Rossner H H and Krappe H J 2007 *Phys. Rev.* B **76** 014301
[37] Quong A A 1994 *Phys. Rev.* B **49** 3226
[38] Lynn J W, Smith H G and Nicklow R M 1973 *Phys. Rev.* B **8** 3493
[39] Synececk V, Chessin H and Simerska M 1970 *Acta Crystallogr.* A **26** 108
[40] Baria J K 2004 *Chin. J. Phys.* **42** 287
[41] Zoli M, Santoro G, Bortolani V, Maradudin A A and Wallis R F 1990 *Phys. Rev.* B **41** 7507
[42] Bruno J A O, Allan N L, Barron T H K and Turner A D 1998 *Phys. Rev.* B **58** 8416
[43] Haug J, Chasse A, Schneider R, Kruth H and Dubiel M 2008 *Phys. Rev.* B **77** 184115
[44] Beccara S a, Dalba G, Fornasini P, Grisenti R, Pederiva F, Sanson A, Diop D and Rocca F 2003 *Phys. Rev.* B **68** 140301(R)